# FIELDS AND ELEMENTARY PARTICLES

K.A. BUGAEV,[1] D.R. OLIINYCHENKO,[1, 2] V.V. SAGUN,[1] A.I. IVANYTSKYI,[1]
J. CLEYMANS,[3] E.S. MIRONCHUK,[4] E.G. NIKONOV,[5] A.V. TARANENKO,[6]
G.M. ZINOVJEV [1]

[1] Bogolyubov Institute for Theoretical Physics, Nat. Acad. of Sci. of Ukraine
  *(14b, Metrolohichna Str., Kyiv 03680, Ukraine; e-mail: bugaev@th.physik.uni-frankfurt.de)*
[2] FIAS, Goethe-University,
  *(Ruth-Moufang Str. 1, 60438 Frankfurt upon Main, Germany; e-mail: dimafopf@gmail.com)*
[3] Department of Physics, University of Cape Town
  *(Rondebosch 7701, South Africa; e-mail: jean.cleymans@uct.ac.za)*
[4] Moscow Institute of Physics and Technology
  *(Dolgoprudnyi, Moscow Region 141700, Russia)*
[5] Laboratory for Information Technologies, JINR
  *(Dubna 141980, Russia; e-mail: e.nikonov@jinr.ru)*
[6] National Research Nuclear University "Moscow Engineering Physics Institute"
  *(31, Kashirskoe Shosse, Moscow 115409, Russia)*

PACS 25.75.-q, 25.75.Nq

# SEPARATE CHEMICAL FREEZE-OUTS OF STRANGE AND NON-STRANGE HADRONS AND PROBLEM OF RESIDUAL CHEMICAL NON-EQUILIBRIUM OF STRANGENESS IN RELATIVISTIC HEAVY ION COLLISIONS

*We present an elaborate version of the hadron resonance gas model with the combined treatment of separate chemical freeze-outs for strange and non-strange hadrons and with an additional $\gamma_s$ factor which accounts for the remaining strange particle non-equilibration. Within the suggested approach, the parameters of two chemical freeze-outs are connected by the conservation laws of entropy, baryonic charge, third isospin projection, and strangeness. The developed model enables us to perform a high-quality fit of the hadron multiplicity ratios measured at AGS, SPS, and RHIC with $\chi^2/dof \simeq 0.93$. A special attention is paid to a successful description of the Strangeness Horn. The well-known problem of selective suppression of $\bar{\Lambda}$ and $\bar{\Xi}$ hyperons is also discussed. The main result is that, for all collision energies, the $\gamma_s$ factor is about 1 within the error bars, except for the center-of-mass collision energy 7.6 GeV, at which we find about 20% enhancement of strangeness. Also we confirm the existence of strong jumps in the pressure, temperature, and effective number of degrees of freedom at the stage of strange particle chemical freeze-out, when the center-of-mass collision energy changes from 4.3 to 4.9 GeV. We argue that these irregularities may signal about the quark-hadron phase transition.*

*K e y w o r d s: chemical freeze-out, strangeness enhancement/suppression factor $\gamma_s$, Strangeness Horn, hadron multiplicities.*

## 1. Introduction

Relativistic nucleus-nucleus (A + A) collisions provide us with experimental information about the

phase diagram of quantum chromodynamics (QCD) and the strongly interacting matter properties. The last stage of such collisions is traditionally analyzed within the statistical approach, which gives us an excellent opportunity to reveal the parameters of chemical freeze-out. This approach is based on the assumption of the thermal equilibrium existence during the last stage of the A + A reaction. Such an equilibrium can be reached due to the intensive particle scattering. The stage of the evolution, when the inelastic reactions between hadrons in the system stop, is referred to as a chemical freeze-out (FO). Particle yields are determined by the parameters of FO, namely by chemical potentials and temperature. This general picture is a basis of the Hadron Resonance Gas Model (HRGM) [1] which is the most successful one in describing the hadronic yields measured in heavy-ion experiments for energies from AGS to LHC. Despite a significant success of the HRGM, there are a few unresolved problems in the analysis of experimental data. In general, they are related to the description of hadron yields which contain (anti)strange quarks. Thus, the energy dependence of $K^+/\pi^+$ and $\Lambda/\pi^-$ ratios remained out of a high-quality description for almost a decade. The excess of strange hadrons yields within the HRGM led the physical community to ponder over the strangeness suppression in heavy ion collisions. The first receipt to resolve this problem was to introduce the strangeness suppression factor $\gamma_s$ which should be fitted in order to describe the experimental data [2]. However, such an approach is not supported by any underlying physical model, and the physical meaning of $\gamma_s$ remains unclear [1, 3–8]. In addition, the strangeness suppression approach in its original form does not contain a hard-core repulsion between hadrons, while the latter is an important feature of the HRGM. A significant role of the hard-core repulsion was demonstrated once more in Ref. [5] where the global fit of hadron yield ratios was essentially improved (to $\chi^2/\text{dof} \simeq 1.16$), as compared to all previous analyses.

The most advanced way to account for the hard-core repulsion between hadrons is to consider a hadron gas as a multicomponent mixture of particles with different hard-core radii [4–7, 9, 10]. Within this approach, all baryons and mesons except for the kaons and the pions are endowed by the common hard-core radii $R_b$ and $R_m$, respectively. At the same time, the kaon and the pion radii $R_K$ and $R_\pi$ are

fitted independently in order to provide the best description of $K^+/\pi^+$ ratio [5]. This is an important finding since the non-monotonic energy dependence of $K^+/\pi^+$ ratio may indicate some qualitative changes of properties of the system and may serve as a signal of the deconfinement onset. This is a reason why such a ratio known as the Strangeness Horn is of a special interest. Note that the multicomponent approach substantially increased the Strangeness Horn description quality, without spoiling the other ratios including $\Lambda/\pi^-$ one. However, even this advanced approach does not reproduce the topmost point of the Strangeness Horn indicating that the data description is still not ideal. In order to resolve this problem, the $\gamma_s$ factor was considered in Ref. [7] as a free parameter within the HRGM with multicomponent repulsion. Although the $\gamma_s$ data fit sizably improves the quality of a Strangeness Horn description, it does not seem to be useful for the description of other hadron multiplicities [7,9]. Furthermore, in contrast to the claims established on the low-quality fit [11], it was found [7] at low energies that, within the error bars in heavy ion collisions, there is a strangeness enhancement, i.e. $\gamma_s > 1$, and not a suppression. The strangeness enhancement was confirmed very recently [12] by the high-quality fit of the available data within the multicomponent HRGM/ in which the hard-core radius of a $\Lambda$ (anti)hyperon was considered as a global fitting parameter in addition to the set of hard-core radii used in [4–7, 9].

However, the effect of apparent strangeness non-equilibration can be more successfully explained by the hypothesis of separate chemical FO for all strange hadrons. Since all the hadrons made of $u$ and $d$ quarks are under thermal equilibration, whereas the hadrons containing $s$ quark are not, it is reasonable to assume two different FOs for these two kinds of particles. Following this conclusion, a separate strangeness FO (SFO) was introduced in Ref. [7,8]. Note that, according to [7], both FO and SFO parameters are connected by the conservation laws of entropy, baryonic charge, and isospin projection, while the net strangeness is explicitly set to zero at FO and at SFO. These conservation laws are crucial elements of the concept of separate SFO developed in [7], which allows one to essentially reduce the number of independent fitting parameters. Another principal element that differs the HRGM of [7,9] from the ideal gas treatment

used in [8, 13] is the presence of a multicomponent hard-core repulsion.

Using the HRGM of [7], it is possible to successfully describe all hadron multiplicities measured in A + A collisions at AGS, SPS, and RHIC energies with $\chi^2/\text{dof} \simeq 1.06$. The concept of separate SFO led to a systematic improvement of the description of all experimental data. However, the topmost point of the Strangeness Horn again was not fitted even within the experimental error, although the general description of $K^+/\pi^+$ ratio energy dependence was rather good except for the upper point.

Since the introduction of the $\gamma_s$ factor demonstrated a remarkable description of all points of the Strangeness Horn, whereas the separate SFO led to a systematic improvement of all hadron yields description, we decided to combine these elements in order to describe an experimental data with the highest possible quality. In this way, we would like to examine the problem whether the concept of separate SFO is able to completely explain a possible non-equilibrium of strange charge, and whether there exist a necessity on the top of the SFO to employ the $\gamma_s$ factor in the statistical approach. Note that, from the academic point of view, the problem of residual strangeness non-equilibration, i.e. the question whether the strange charge is or is not in the full chemical equilibrium, is of principal importance. This ambitious task is the main goal of the present paper. Evidently, the best tool for such a purpose is the most successful version of the HRGM, i.e. the HRGM with the multicomponent hadronic repulsion and a separate SFO. As it will be shown below, such an approach allows us to describe 111 independent hadron yield ratios measured for 14 values of the center-of-mass collision energy $\sqrt{s_{NN}}$ in the interval from 2.7 GeV to 200 GeV with very high quality.

The paper is organized as follows. The basic features of the developed model are outlined in Section 2, while the fitting procedure of the present model is outlined in Section 3. The main obtained results are compared with the other models in Section 4. In Section 5, we discuss the new fit of hadronic multiplicity ratios with two chemical freeze-outs and $\gamma_s$ factor in detail, while Section 6 contains our conclusions.

## 2. Model Description

In what follows, we treat a hadronic system as a multicomponent Boltzmann gas of hard spheres. The ef-

fects of quantum statistics are negligible for typical temperatures of the hadronic gas, whereas the hard-core repulsion between the particles significantly affects a corresponding equation of state [5, 10]. The present model is dealing with the Grand Canonical treatment. Hence a thermodynamic state of system under consideration is fixed by the volume $V$, the temperature $T$, the baryonic chemical potential $\mu_B$, the strange chemical potential $\mu_S$, and the chemical potential of the isospin third component $\mu_{I3}$. These parameters control the pressure $p$ of the system. In addition, they define the densities $\rho_i^K$ of corresponding charges $Q_i^K$ ($K \in \{B, S, I3\}$). Introducing the symmetric matrix of the second virial coefficients $b_{ij} = \frac{2\pi}{3}(R_i + R_j)^3$, we can obtain the parametric equation of state of the present model in a compact form

$$p = \sum_{i=1}^{N} p_i, \quad \rho_i^K = \frac{Q_i^K p_i}{T + \frac{\sum_{jl} p_j b_{jl} p_l}{p}}, \qquad (1)$$

using the partial pressure $p_i$ of the $i$-th sort of particles. The equation of state is written in terms of the solutions $p_i$ of the system

$$p_i = T\phi_i(T) \exp\left[\frac{\mu_i - 2\sum_j p_j b_{ji} + \sum_{jl} p_j b_{jl} p_l/p}{T}\right], \quad (2)$$

$$\phi_i(T) = \frac{g_i}{(2\pi)^3} \int \exp\left(-\frac{\sqrt{k^2 + m_i^2}}{T}\right) d^3k. \qquad (3)$$

Each $i^{\text{th}}$ sort is characterized by its full chemical potential $\mu_i = Q_i^B \mu^B + Q_i^S \mu^S + Q_i^{I3} \mu^{I3}$, mass $m_i$, and degeneracy $g_i$. The function $\phi_i(T)$ denotes the corresponding particle thermal density in case of ideal gas. The obtained model parameters for two freeze-outs and their dependence on the collision energy are discussed in the next section. They are obtained for the following values of hard-core radii, which were determined earlier in [5, 7]: $R_\pi = 0.1$ fm for pions, $R_K = 0.38$ fm for kaons, $R_m = 0.4$ fm for all other mesons and $R_b = 0.2$ fm for all baryons.

In order to account for the possible strangeness non-equilibration, we introduce the $\gamma_s$ factor in a conventional way, by replacing $\phi_i$ in Eq. (2) as

$$\phi_i(T) \to \phi_i(T)\gamma_s^{s_i}, \qquad (4)$$

where $s_i$ is the number of strange valence quarks plus the number of strange valence antiquarks.

The principal difference of the present model from the traditional approaches is that we employ an independent chemical FO of strange particles. Let us consider this in some details. The independent FO of strangeness means that inelastic reactions (except for the decays) with hadrons made of s quarks are switched off at the temperature $T_{\mathrm{SFO}}$, the baryonic chemical potential $\mu_{B_{\mathrm{SFO}}}$, the strange chemical potential $\mu_{S_{\mathrm{SFO}}}$, the isospin third projection chemical potential $\mu_{I3_{\mathrm{SFO}}}$, and the three-dimensional emission volume $V_{\mathrm{SFO}}$. In the general case, these parameters of SFO do not coincide with the temperature $T_{\mathrm{FO}}$, the chemical potentials $\mu_{B_{\mathrm{FO}}}$, $\mu_{S_{\mathrm{FO}}}$, $\mu_{I3_{\mathrm{FO}}}$, and the volume $V_{\mathrm{FO}}$, which characterize the FO of non-strange hadrons. The particle yields are given by the charge density $\rho_i^K$ in (1) and the corresponding volume at FO and at SFO.

At the first glance, a model with independent SFO contains four extra fitting parameters for each energy value as compared to the traditional approach (temperature, three chemical potentials, and the volume at SFO instead of the strangeness suppression/enhancement factor $\gamma_s$). However, this is not the case due to the conservation laws. Indeed, since the entropy, the baryonic charge, and the isospin third projection are conserved, the parameters of FO and SFO are connected by the following equations:

$$s_{\mathrm{FO}}V_{\mathrm{FO}} = s_{\mathrm{SFO}}V_{\mathrm{SFO}},\tag{5}$$
$$\rho^B_{\mathrm{FO}}V_{\mathrm{FO}} = \rho^B_{\mathrm{SFO}}V_{\mathrm{SFO}},\tag{6}$$
$$\rho^{I_3}_{\mathrm{FO}}V_{\mathrm{FO}} = \rho^{I_3}_{\mathrm{SFO}}V_{\mathrm{SFO}},\tag{7}$$

where the entropy density $s_A = \frac{\partial p}{\partial T}\big|_A$, the density of baryonic charge $\rho_A^B = \frac{\partial p}{\partial \mu^B}\big|_A$, and the density of the isospin third projection $\rho_A^{I3} = \frac{\partial p}{\partial \mu^{I3}}\big|_A$ are found from the usual thermodynamic identities at SFO (A = SFO) or at FO (A = FO).

The effective volumes can be excluded, if these equations are rewritten as

$$\frac{s}{\rho^B}\bigg|_{\mathrm{FO}} = \frac{s}{\rho^B}\bigg|_{\mathrm{SFO}}, \qquad \frac{\rho^B}{\rho^{I_3}}\bigg|_{\mathrm{FO}} = \frac{\rho^B}{\rho^{I_3}}\bigg|_{\mathrm{SFO}}.\tag{8}$$

Thus, the baryonic $\mu_{B_{\mathrm{SFO}}}$ and the isospin third projection $\mu_{I3_{\mathrm{SFO}}}$ chemical potentials at SFO are now defined by Eqs. (8). Note that the strange chemical potentials $\mu_{S_{\mathrm{FO}}}$ and $\mu_{S_{\mathrm{SFO}}}$ are found from the condition of vanishing the net strangeness at FO and SFO, respectively. Therefore, the concept of independent

SFO leads to an appearance of one independently fitting parameter $T_{\mathrm{SFO}}$. Hence, the independent fitting parameters are the following: the baryonic chemical potential $\mu_B$, the chemical potential of the third projection of isospin $\mu_{I3}$, the chemical freeze-out temperature for strange hadrons $T_{\mathrm{SFO}}$, the chemical freeze-out temperature for all non-strange hadrons $T_{\mathrm{FO}}$, and the $\gamma_s$ factor (i.e. 5 fitting parameters for each collision energy).

An inclusion of the width $\Gamma_i$ of hadronic states is an important element of the present model. It is due to the fact that the thermodynamic properties of the hadronic system are sensitive to the width [5,7,14]. In order to account for the finite width of resonances, we perform the usual modification of the thermal particle density $\phi_i$. Namely, we convolute the Boltzmann exponent under the integral over momentum with the normalized Breit–Wigner mass distribution. As a result, the modified thermal particle density of the $i^{\mathrm{th}}$ sort of hadrons acquires the form

$$\int \exp\left(-\frac{\sqrt{k^2 + m_i^2}}{T}\right) d^3k \rightarrow$$
$$\rightarrow \frac{\int_{M_0}^{\infty} \frac{dx}{(x-m_i)^2 + \Gamma_i^2/4} \int \exp\left(-\frac{\sqrt{k^2 + x^2}}{T}\right) d^3k}{\int_{M_0}^{\infty} \frac{dx}{(x-m_i)^2 + \Gamma_i^2/4}}.\tag{9}$$

Here, $m_i$ denotes the mean mass of hadrons, and $M_0$ stands for the threshold in the dominant decay channel. The main advantages of this approximation is a simplicity of its realization and a clear way to account for the finite width of hadrons. It is appropriate here to mention that one could use other prescriptions to account for the width of resonances. However, in a recent work [14], it was shown that the Breit–Wigner prescription (9) can provide somewhat better (about 20%) quality of the fit than the Gaussian attenuation of the resonance mass and essentially better one compared to the case without accounting for the width. At the same time, it was found in [14] that, within the error bars, such FO parameters as the temperature, chemical potentials, and $\gamma_s$ factor are the same for different prescriptions of the resonance width accounting. Indeed, it is reasonable to expect that other physically motivated ways to account for the resonance width should give similar results. Therefore, in this work, we will employ the prescription (9), which provides the better description of the data.

The observed hadronic multiplicities contain the thermal and decay contributions. For example, a major part of pions is produced by the decays of heavier hadrons. Therefore, the total multiplicity is obtained as a sum of thermal and decay multiplicities, exactly as it is done in a conventional model. However, writing the formula for final particle densities, we have to take into account that the FO and SFO volumes can be different:

$$\frac{N^{\text{fin}}(X)}{V_{\text{FO}}} = \sum_{Y \in \text{FO}} BR(Y \to X)\rho^{\text{th}}(Y) +$$

$$+ \sum_{Y \in \text{SFO}} BR(Y \to X)\rho^{\text{th}}(Y)\frac{V_{\text{SFO}}}{V_{\text{FO}}}. \qquad (10)$$

Here, the first term on the right-hand side is due to decays after FO, whereas the second one accounts for the strange resonances decayed after SFO. The factor $V_{\text{SFO}}/V_{\text{FO}}$ can be replaced by $\rho^{B}_{\text{FO}}/\rho^{B}_{\text{SFO}}$ due to the baryonic charge conservation. $BR(Y \to X)$ denotes the branching ratio of the Y-th hadron decay into the X-th hadron, with the definition $BR(X \to X) = 1$ used for the sake of convenience. The input parameters of the present model (masses $m_i$, widths $\Gamma_i$, degeneracies $g_i$, and branching ratios of all strong decays) were taken from the particle tables of the thermodynamical code THERMUS [15].

## 3. Fitting Procedures

**Data sets**. The present model is applied to fit the data. We take the ratios of particle multiplicities at mid-rapidity as the data points. In contrast to fitting multiplicities themselves, such an approach allows us to cancel the possible experimental biases. In this paper, we use the data set almost identical to Ref. [7]. At the AGS energies ($\sqrt{s_{NN}} = 2.7$–4.9 AGeV or $E_{\text{lab}} = 2$–10.7 AGeV) the data are available with a good energy resolution above 2 AGeV. However, for the beam energies 2, 4, 6, and 8 AGeV, only a few data points are available. They corresponds to the yields for pions [16, 17], for protons [18, 19], and for kaons [17] (except for 2 AGeV). The data integrated over $4\pi$ are also available for $\Lambda$ hyperons [20] and for $\Xi^-$ hyperons (for 6 AGeV only) [22]. However, as was argued in Ref. [1], the data for $\Lambda$ and $\Xi^-$ should be recalculated for mid-rapidity. Therefore, instead of raw experimental data, we used the corrected values from [1]. Next comes the data set at the highest AGS energy ($\sqrt{s_{NN}} = 4.9$ AGeV or

$E_{\text{lab}} = 10.7$ AGeV). Similarly to [5], we analyze here only the NA49 mid-rapidity data [23–28]. Since the RHIC high-energy data of different collaborations agree with each other, we analyzed the STAR results for $\sqrt{s_{NN}} = 9.2$ GeV [29], $\sqrt{s_{NN}} = 62.4$ GeV [30], $\sqrt{s_{NN}} = 130$ GeV [31–34] and $\sqrt{s_{NN}} = 200$ GeV [34–36].

**Combined fit with SFO and $\gamma_s$ factor.** A comprehensive data analysis [7] performed recently for two alternative approaches, i.e the first one with $\gamma_s$ as a free parameter and the second one with separate FO and SFO, showed the advantages and disadvantages of both methods. Thus, the $\gamma_s$ fit provides one with an opportunity to noticeably improve the Strangeness Horn description with $\chi^2/\text{dof} = 3.3/14$, comparably to the previous result $\chi^2/\text{dof} = 7.5/14$ [5], but there are only slight improvements of the ratios with strange baryons (global $\chi^2/\text{dof} : 1.16 \to 1.15$). The obtained results for the SFO approach demonstrate a high fit quality for the most problematic ratios for the HRGM, especially for $\bar{p}/\pi^-$, $\bar{\Lambda}/\Lambda$, $\bar{\Xi}^-/\Xi^-$, and $\bar{\Omega}/\Omega$. Although the overall $\chi^2/\text{dof} \simeq 1.06$ is notably better than with the $\gamma_s$ factor [5, 7], the description of the Horn's highest point got worsen. These results led us to an idea to investigate the combination of these two approaches in order to get the high-quality Strangeness Horn description without spoiling the quality of other particle ratios. However, we immediately face a mathematical problem to justify such a combined fit because, at six values of the center-of-mass collision energies, namely $\sqrt{s_{NN}} = 2.7, 3.3, 3.8, 4.3, 9.2, 62.4$ GeV, the number of independent hadron yield ratios (4, 5, 5, 5, 5, 5, respectively) is equal or even smaller than the number of fitting parameters (see Table 1). For these energies, one can treat, of course, the experimental ratios as equations and can solve them, but, unfortunately, the experimental ratios always have finite (and not small!) error bars. As a result, solving the ratios as equations with finite errors leads to rather large region of chemical FO parameters, which provide a vanishing value of $\chi^2$. Hence, it is hard to conclude what values are the most probable ones. It seems that these difficulties prevented the authors of a recent work [13] to analyze the data at the collision energies $\sqrt{s_{NN}} \leq 4.9$ GeV within their version of the SFO concept [8].

Moreover, in some cases, the range of chemical FO parameters obtained by such a fit, the SFO $\oplus \gamma_S$ hereafter, is located far away from the ones found by the

well-established fit procedures, i.e. by the single FO model without [5] or with [7] the $\gamma_s$ fit and by the SFO with $\gamma_s = 1$ [7], which provide us with very good descriptions of the data. Moreover, all these results are in a very good correspondence with each other. Therefore, the combined SFO and $\gamma_S$ fit can be directly performed for the collision energies $\sqrt{s_{NN}} = 4.9$, 6.3, 7.6, 8.8, 12, 17, 130, 200 GeV only, while, for other energies, we have to seek for another minimization criterion.

Since the major task of the present work is to determine the residual effect of the strangeness nonequilibrium on top of the SFO, it would be reasonable to fix the parameters of the SFO and make the $\gamma_s$ fit. Unfortunately, in this case, the number of degrees of freedom will be the same as for the SFO $\oplus \gamma_S$ fit, i.e. dof = 41, and the resulting value of $\chi^2/$dof

*Table 1.* **The fit results of different versions of the HRGM are compared for 14 values of the center-of-mass collision energies: the column $\chi_1^2$ corresponds to a single FO model of [5]; the column $\chi_2^2$ is found for the SFO with $\gamma_s = 1$ [7]; the column $\chi_3^2$ corresponds to the SFO $+ \gamma_s$ fit with added data points for $N_{rat} \leq 5$, while the column $\chi_4^2$ is obtained by the direct SFO $\oplus \gamma_S$ fit. $N_{rat}$ indicates the available number of independent hadronic ratios at the given center-of-mass collision energy $\sqrt{s_{NN}}$. In the row Sum we list the sum of the $i$-th column, while, in the bottom row, the number of degrees of freedom of each HRGM version is shown (for more details, see the text)**

| $\sqrt{s_{NN}}$ (GeV) | $\chi_1^2$ FO | $N_{rat}$ | $\chi_2^2$ SFO | $\chi_3^2$ SFO $+ \gamma_S$ | $\chi_4^2$ SFO $\oplus \gamma_S$ |
|---|---|---|---|---|---|
| 2.7 | 0.62 | 4 | 0.62 | 0.62 | $1.3 \times 10^{-5}$ |
| 3.3 | 0.17 | 5 | 0.08 | 0.08 | $3.4 \times 10^{-9}$ |
| 3.8 | 0.56 | 5 | 0.03 | 0.03 | 0.03 |
| 4.3 | 0.35 | 5 | 0.26 | 0.26 | 0.21 |
| 4.9 | 0.55 | 8 | 0.55 | 0.40 | 0.40 |
| 6.3 | 7.91 | 9 | 2.88 | 2.45 | 2.45 |
| 7.6 | 17.5 | 10 | 16.6 | 5.9 | 5.9 |
| 8.8 | 7.9 | 11 | 7.85 | 7.56 | 7.56 |
| 9.2 | 0.16 | 5 | 0.15 | 0.03 | $1.3 \times 10^{-7}$ |
| 12 | 17.3 | 10 | 11.9 | 9.57 | 9.57 |
| 17 | 14.7 | 13 | 7.39 | 7.38 | 7.38 |
| 62.4 | 0.4 | 5 | 0.09 | 0.03 | 0.03 |
| 130 | 5 | 11 | 4.62 | 4.32 | 4.32 |
| 200 | 7.4 | 10 | 5.49 | 5.09 | 5.09 |
| Sum | 80.5 | 111 | 58.5 | 43.72 | 42.9 |
| Dof | 69 | N/A | 55 | 47 | 41 |

would not be better than the one obtained within the SFO $\oplus \gamma_S$ fit. Hence, to avoid the above-mentioned problems, we suggest to modify the definition of $\chi^2$ for the six values of the collision energy, which have 5 or less independent ratios

$$\chi^2 = \sum_i \frac{(r_i^{\text{theor}} - r_i^{\text{exp}})^2}{\sigma_i^2} +$$
$$+ \left[ \frac{T_{\text{SFO}} - T_{\text{SFO}}(\gamma_s = 1)}{\sigma_T^{\text{SFO}}} \right]^2, \tag{11}$$

where $r_i^{\text{theor}}$ and $r_i^{\text{exp}}$ are, respectively, the theoretical and experimental values of particle yields ratios, $\sigma_i$ stands for the corresponding experimental error, and the summation is performed over all experimental points, which are available at the considered energy. Here, $\sigma_T^{\text{SFO}}$ denotes the error of the SFO temperature $T_{\text{SFO}}(\gamma_s = 1)$, which is found for each problematic energy by the SFO fit with $\gamma_s = 1$, while the chemical FO temperature of strange particles $T_{\text{SFO}}$ is the fitting parameter.

In other words, for each of the energies corresponding to a set of problematic ratios, we suggest to consider the SFO temperature $T_{\text{SFO}}(\gamma_s = 1)$, as an additional datum to be fitted within the combined SFO $+ \gamma_s$ approach, while, for other collision energies, we used the standard definition $\chi^2 = \sum_i \frac{(r_i^{\text{theor}} - r_i^{\text{exp}})^2}{\sigma_i^2}$ for the combined fit. In order to distinguish this approach from the SFO $\oplus \gamma_S$ fit, we refer to it as the SFO $+ \gamma_s$ fit. Such a reformulation of the minimization criterion for $\sqrt{s_{NN}} =$ 2.7, 3.3, 3.8, 4.3, 9.2, 62.4 GeV allows us to avoid the mathematical problems of the combined SFO $\oplus \gamma_s$ fit and to simultaneously keep the temperature of strange particles $T_{\text{SFO}}$ not far away from the SFO temperature $T_{\text{SFO}}$. Originally, for $\sqrt{s_{NN}} = 2.7$, we added two data points into the $\chi^2$ definition (11) in order to have 6 data for 5 fitting parameters, but then we found that adding one data point is sufficient, since it resolves the problem.

## 4. Main Results

The results of the SFO $+ \gamma_s$, SFO $\oplus \gamma_S$, and SFO fits are compared for $\sqrt{s_{NN}} = 2.7$ and 3.3 GeV in Fig. 1 (for more details, see also Table 1). As one can see from this figure, the SFO description is already very good ($\chi^2 \equiv \chi_2^2 \simeq 0.62$ in Table 1). Hence, the additional parameter $\gamma_s$ cannot improve it (compare $\chi_3^2$ and $\chi_2^2$ in Table 1), if the number of data points is

equal or larger than the number of fitting parameters. Thus, the mathematically justified SFO + $\gamma_s$ fitting procedure does not improve the description quality compared to the SFO fit at these collision energies. Hence, we find that $\gamma_s \simeq 1$ within the error bars. Moreover, for a completeness, we used another way of fitting: first, we determined the parameters of two chemical freeze-out within the SFO model with $\gamma_s = 1$ (see the $\chi_2^2$ column in Table 1), fixed the found parameters, and then performed the fitting of the $\gamma_s$ parameter. It is remarkable that, in this way, we did not get any improvement of the fit quality compared to the SFO + $\gamma_s$ fit and got the same FO temperatures and chemical potentials as in the latter case not only for the problematic data points, but, within the error bars, we found the same results for all other energies of collision.

The main results for the SFO $\oplus \gamma_S$, and SFO + $\gamma_s$ fits found here are as follows. Due to the problems discussed above, the SFO $\oplus \gamma_S$ model does not allow us to locate the narrow region of the chemical FO parameters for the collision energies $\sqrt{s_{NN}} = 2.7$, $3.3$ and $9.2$ GeV, while, for the energies $\sqrt{s_{NN}} = 3.8$, $4.3$, and $62.4$ GeV, we did not find the solutions of five equations for five variables and, hence, were able to perform the usual minimization of $\chi^2$.

The SFO $\oplus \gamma_S$ model gives $\chi_4^2/\mathrm{dof} = 42.96/41 \simeq \simeq 1.05$, which is only a very slight improvement compared to the previously obtained results for the SFO model $\chi_2^2/\mathrm{dof} = 58.5/55 \simeq 1.06$. The redefinition of the $\chi^2$ criterion (11) allows us to avoid the mathematical problems within the SFO + $\gamma_s$ model and to sizably reduce the $\chi^2$ value per degree of freedom to $\chi_3^2/\mathrm{dof} = 43.72/47 \simeq 0.93$. Moreover, for the problematic data at the collision energies $\sqrt{s_{NN}} = 3.8$, $4.3$, and $62.4$ GeV within the SFO + $\gamma_s$ model, we obtained practically the same chemical FO parameters and the same quality of the fit (compare the values of $\chi_3^2$ and $\chi_4^2$ in Table 1 for these energies), as for the SFO $\oplus \gamma_S$ model, including the main conclusion that $\gamma_s \simeq 1$ (see the upper panel of Fig. 2). Such a result provides an additional justification for the $\chi^2$ criterion redefinition (11).

Nevertheless, as one can see from Table 1 compared to the SFO model with $\gamma_s = 1$ (see the column with $\chi_2^2$), the main reduction of $\chi^2$ achieved by the $\gamma_S$ parameter corresponds to $\sqrt{s_{NN}} = 7.6$ GeV, i.e this is exactly where the Strangeness Horn peak is located. Moreover, we found that the fitting results
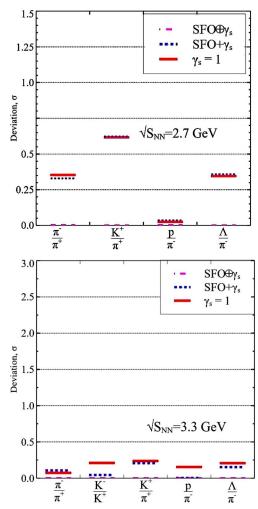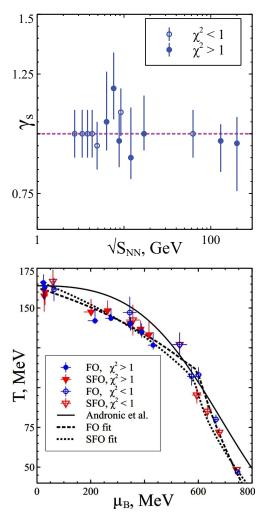


**Fig. 1.** (Colour on-line) Relative deviation of the theoretical description of ratios from the experimental value in units of the experimental error $\sigma$. Particle ratios vs. the modulus of relative deviation ($\frac{|r^{\mathrm{theor}} - r^{\mathrm{exp}}|}{\sigma^{\mathrm{exp}}}$) for $\sqrt{s_{NN}} = 2.7$ and $3.3$ GeV are shown. Solid lines correspond to the model with a single FO of all hadrons and $\gamma_s = 1$, the dotted lines correspond to the model SFO + $\gamma_s$, as explained in the text. The results of the SFO $\oplus \gamma_s$ model are indicated by the dashed lines

can be separated into two distinct groups: those, where $\chi^2 > 1$ and where $\chi^2 < 1$ for any of our fits. It is remarkable that neither SFO, nor $\gamma_s$ fits do not move any of the points of one group to another group. If, for a certain collision energy, the inequality $\chi^2 > 1$ occurred, then it always holds after any of our efforts. The results obtained for the SFO + $\gamma_s$ are shown in Figs. 2–10. Note that, compared to the SFO model with $\gamma_s = 1$ [7], the value of $\chi^2$ itself for
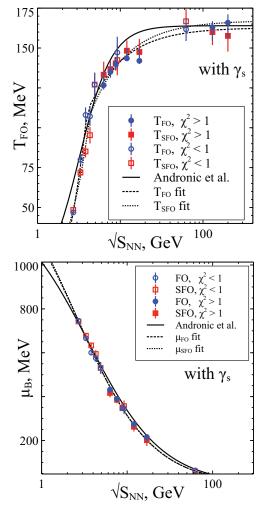
**Fig. 2.** (Colour on-line) *Upper panel:* $\sqrt{s_{NN}}$ dependence of the $\gamma_s$ factor within the SFO$+\gamma_S$ model with two freeze-outs and the $\gamma_s$ fit. *Lower panel:* Chemical freeze-outs parameters found within the SFO$+\gamma_s$ model. Baryonic chemical potential dependence of the chemical freeze-out temperature for the strange hadrons (SFO points are marked with triangles) and for the non-strange ones (FO points are marked with circles). The pairs of nearest points are connected by the isentrops $s/\rho_B = \text{const}$, on which the FO and the SFO points are located

**Fig. 3.** (Colour on-line) Behavior of the SFO$+\gamma_S$ model parameters: the chemical freeze-out temperatures $T_{\rm FO}$ and $T_{\rm SFO}$ vs. $\sqrt{s_{NN}}$ (upper panel) and the freeze-out baryonic chemical potentials $\mu_B^{\rm FO}$ and $\mu_B^{\rm SFO}$ vs. $\sqrt{s_{NN}}$ (lower panel)

the SFO$+\gamma_S$ fit, not divided by number of degrees of freedom, has improved notably, although the deviation of the $\gamma_s$ factor from 1 does not exceed 20% even for the topmost point of the Strangeness Horn (see the upper panel of Fig. 2). Note that our results on the SFO$+\gamma_S$ model are very similar to the SFO model of Ref. [13] (just compare our Fig. 3 with Fig. 4 in [13]), although, at the energies $\sqrt{s_{NN}} = 130$ GeV

and $\sqrt{s_{NN}} = 200$ GeV, we find that the temperature of FO is slightly higher than the temperature of SFO, while the situation is opposite in [13]. Two possible reasons for such a difference is that, in Ref. [13], the conservation laws (5)–(7) are ignored, and their treatment is based on the ideal gas picture. As a result, the fit quality achieved in [13] is essentially lower (see Fig. 5 in there) compared to the present work.

It is remarkable that the present rather sophisticated fit of the hadronic multiplicities confirms the recent finding on the non-smooth behavior of the function $T_{\rm FO}(\mu_B^{\rm FO})$ reported in [14] for the same hard-core radius of hadrons $R = 0.3$ fm. A simi-

lar change of the slope of $T_{\mathrm{SFO}}(\mu_B^{\mathrm{SFO}})$ occurring at the collision energy $\sqrt{s_{NN}} \simeq 4$ GeV is a new result shown in Fig. 2. Following work [14], we parametrize $T_{\mathrm{FO}}(\sqrt{s_{NN}})$, $T_{\mathrm{SFO}}(\sqrt{s_{NN}})$, $\mu_B^{\mathrm{FO}}(\sqrt{s_{NN}})$, and $\mu_B^{\mathrm{SFO}}(\sqrt{s_{NN}})$ as

$$T = (T_1 + T_2\sqrt{s_{NN}}) \cdot c_+(\sqrt{s_{NN}}, 4.0, 0.1) +$$
$$+ (T_3/\sqrt{s_{NN}} + T_4) \cdot c_-(\sqrt{s_{NN}}, 4.0, 0.1), \quad (12)$$

$$\mu_B = \frac{A}{1 + B\sqrt{s_{NN}}}, \quad (13)$$

where $c_\pm(x, a, b)$ are the sigmoid functions

$$c_+(x, a, b) = \frac{1}{1 + e^{(x-a)/b}} = \frac{1}{2}\left(1 - \tanh\frac{x-a}{2b}\right), (14)$$

$$c_-(x, a, b) = \frac{1}{1 + e^{(a-x)/b}} = \frac{1}{2}\left(1 + \tanh\frac{x-a}{2b}\right). (15)$$

The main reason to employ parametrizations (12)–(15) is a drastic change of the $\sqrt{s_{NN}}$ dependence of the function $T_{\mathrm{FO}}(\sqrt{s_{NN}})$ in the narrow region $\sqrt{s_{NN}} \simeq 4.3$–$4.9$ GeV found in [14]. The upper panel of Fig. 3 confirms that a similar behavior of $T_{\mathrm{FO}}(\sqrt{s_{NN}})$ and $T_{\mathrm{SFO}}(\sqrt{s_{NN}})$ exists within the SFO $+ \gamma_s$ model, although the switch value of the collision energy $\sqrt{s_{NN}} \simeq 4$ GeV is about ten percents lower than the one found for the single FO model of work [14]. The resulting curves (12) and (13) for the SFO $+ \gamma_s$ model are shown in Fig. 3, whereas the corresponding parameters are given in Table 2. Using curves (12) and (13), we obtained the analytic expressions for the functions $T_{\mathrm{FO}}(\mu_B^{\mathrm{FO}})$ and $T_{\mathrm{SFO}}(\mu_B^{\mathrm{SFO}})$, which are shown in the lower panel of Fig. 2.

For a comparison, we depict the parametrization of the chemical freeze out temperature ($\sqrt{s_{NN}}$ is given in GeVs) in Figs. 2 and 3,

$$T^{\mathrm{FO}}[\mathrm{MeV}] = \frac{T^{\mathrm{lim}}}{1 + \exp\left[2.60 - \ln(\sqrt{s_{NN}})/0.45\right]} =$$
$$= T^{\mathrm{lim}} c_-(\ln(\sqrt{s_{NN}}), 1.17, 0.45), \quad (16)$$

which together with parametrization (13) was suggested in [1]. The parameters $T^{\mathrm{lim}} = 164$ MeV, $A = 1303$ MeV, $B = 0.286$ GeV$^{-1}$ were found in [3]. Although they have close values to $T_4$, $A$, and $B$ listed in Table, only the curves $\mu_B(\sqrt{s_{NN}})$ found here and in [3] look similar (see the lower panel of Fig. 3). From the upper panel of Fig. 3, one can see that curves (12) and (16) have rather different behaviors at the low and intermediate values of collision energy. As a result, the functions $T_{\mathrm{FO}}(\mu_B^{\mathrm{FO}})$ found here and in [3]
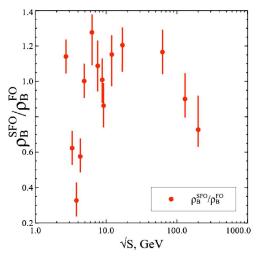


***Fig. 4.*** (Colour on-line) $\sqrt{s_{NN}}$ dependence of the ratio of baryonic charge densities at SFO and at FO within the SFO $+ \gamma_S$ model. Since the baryonic charge is conserved, such a ratio coincides with the inverse ratio of corresponding freeze-out volumes, i.e. with $V_{\mathrm{FO}}/V_{\mathrm{SFO}}$

have different shapes, as one can see from the lower panel of Fig. 2. We have to note that our efforts to reasonably describe the FO and SFO temperatures by the parametrization (16) were not successful, and the corresponding values of $\chi^2/\mathrm{dof}$ were almost one order of magnitude larger than the ones given in Table 2 for Eq. (12). Clearly, the found parametrizations should be considered as the predictions for the chemical FO and SFO characteristics, which can be experimentally tested at the accelerators FAIR (GSI, Darmstadt) and NICA (JINR, Dubna).

In Fig. 4, we show the ratio of baryonic charge densities at SFO and at FO within the SFO $+ \gamma_S$ model, which coincides with the inverse ratio of corre-

*Table 2.* **The parameters of Eqs. (12) and (13) found from fitting the values of chemical freeze out parameters of the SFO $+ \gamma_s$ model**

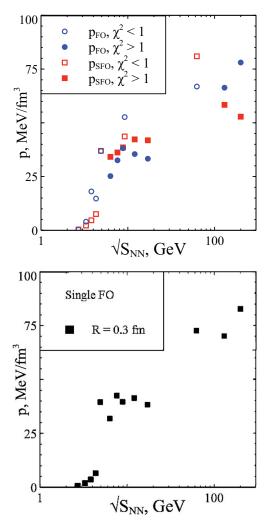|  | FO | SFO |
|---|---|---|
| $T_1$ (MeV) | −82.7 | −43.9 |
| $T_2$ (MeV) | 48.1 | 34.2 |
| $T_3$ MeV) | −211.8 | −254.8 |
| $T_4$ (MeV) | 162.8 | 167.2 |
| $\chi^2/\mathrm{dof}$ fit Eq. (12) | 16/9 | 14.5/9 |
| $A$ (MeV) | 1501 | 1525 |
| $B$(GeV$^{-1}$) | 0.38 | 0.39 |
| $\chi^2/\mathrm{dof}$ fit Eq. (13) | 3.4/12 | 8.1/12 |

**Fig. 5.** (Colour on-line) $\sqrt{s_{NN}}$ dependences of the pressure at FO and SFO points found within the SFO $+ \gamma_s$ model (upper panel) and within a single FO model for the same hard-core radius $R = = 0.3$ fm of all hadrons [14]

sponding freeze-out volumes $V_{\rm FO}/V_{\rm SFO}$ due to the baryonic charge conservation. From this figure, one can see that the visually small difference of temperatures and baryonic chemical potentials at SFO and FO leads, nevertheless, to quite sizable differences of other thermodynamic quantities. As one can see from the upper panel of Fig. 5, this is also true for the pressure existing at SFO and at FO.

In addition, we confirm the existence of irregularities in the FO pressure found earlier [14]. We find similar irregularities for the SFO pressure and for the effective number of degrees of freedom for SFO,

$p^{\rm SFO}/(T^{\rm SFO})^4$, i.e. for the ratio of SFO pressure to the fourth power of the SFO temperature. From the upper panel of Fig. 5, one can see that the largest increase of the SFO pressure per increase of the center-of-mass energy of collision occurs at $\sqrt{s_{NN}} = 4.3$–$4.9$ GeV. In other words, for about 14% increase of $\sqrt{s_{NN}}$, the SFO pressure increases by 5.3 times, and the ratio $p^{\rm SFO}/(T^{\rm SFO})^4$ increases by about 65%. According to the recent work [41], these and other irregularities observed at chemical FO [14] are signaling about the formation of the mixed quark-gluon-hadron phase, and such an explanation can be experimentally verified in a few years at FAIR and NICA.

One more important finding of the present work can be seen from a comparison of the upper and lower panels of Fig. 5. Note that, in contrast to the temperature or baryonic chemical potential, the pressure allows one easier to distinguish the SFO from FO. Moreover, comparing the squares in the upper and lower panels of Fig. 5, one immediately concludes that the model of a single chemical FO [14] with the same value of hard-core radius for all hadrons describes just the SFO for all values of $\sqrt{s_{NN}}$ below 62.4 GeV. The same is true for a single FO model [5] with different hard-core radii discussed above. This peculiar result can be easily understood, if one recalls that, for the most values of collision energy, the number of ratios involving strange hadrons is essentially larger than the number of ratios with non-strange particles.

At the same time, a single chemical FO model reproduces the FO pressure of the SFO $+ \gamma_s$ model only at $\sqrt{s_{NN}} \geq 62.4$ GeV. The corresponding reasons will be discussed in the next section, while we mention here that, at high RHIC energies, the fit quality of all models, including the single FO one, is rather high, as one can see from Table 1. The main part of $\chi^2$ at these energies is formed by the poor description of $K$-mesons at $\sqrt{s_{NN}} = 62.4$ GeV, $\Lambda$ hyperon at $\sqrt{s_{NN}} = 130$ GeV, and $\Omega^{\pm}$ hyperons at $\sqrt{s_{NN}} = 200$ GeV.

Such a comparison of the single FO model and the SFO $+ \gamma_s$ model pressures allows us to explain a cause of why, in the previous thorough analysis of the particle ratios within the realistic single FO model with the same hard-core radius of hadrons, the main conclusion was that there is no deviation of strange particles from the chemical equilibrium for the mid-rapidity data. In other words, it is possible to naturally explain the reason of why it was found in [1] that, within

the error bars, $\gamma_s \simeq 1$. Our direct comparison of the SFO $+ \gamma_s$ model for the mid-rapidity data shows that the single FO models with the same or different hard-core hadronic radii reproduce the SFO pressure with $\gamma_s \simeq 1$ almost at all collision energies, except for $\sqrt{s_{NN}} = 7.6$ GeV and for $\sqrt{s_{NN}} \geq 62.4$ GeV. In the former case, one finds that $\gamma_s \simeq 1.19$, while, in the latter case, $\gamma_s \simeq 1$. But, as we discussed above, the pressure for high collision energies at FO found within the SFO $+ \gamma_s$ model reproduces the single FO model pressure. Therefore, the main reason for why the chemical non-equilibrium of strange charge was not found within the single FO models is that the fitting procedure mainly described the ratios involving the strange particles and, hence, it would have been more appropriate to consider the chemical non-equilibrium of non-strange hadrons.

## 5. Results for Particle Ratios

The findings discussed above motivate us to study in some details what ratios and at what energies are improved. The most significant improvements correspond to the collision energies $\sqrt{s_{NN}} = 6.3, 7.6,$ and 12 GeV, that are plotted in Figs. 6 and 7. Figures 6 and 7 demonstrate a very high fit quality, especially for such traditionally problematic ratios as $K^+/\pi^+$, $\pi^-/\pi^+$, $\bar{\Lambda}/\pi^-$ and $\varphi/K^+$, which is achieved within the SFO $+ \gamma_S$ model compared to the single FO model and the SFO one. For instance, for $\sqrt{s_{NN}} = 7.6$ GeV, seven ratios out of ten are improved, while, for other energies, the improvements are less significant. On the contrary, the particle ratios measured at $\sqrt{s_{NN}} = 17$ GeV (see Fig. 7) are improved within the SFO model, while the SFO $+ \gamma_S$ fit practically does not lead to any significant improvement compared to the SFO model.

We also found that the SFO $+ \gamma_S$ fit leads to a selective improvement and to a certain degradation of the fit quality of various ratios for different collision energies. For instance, the $\pi^-/\pi^+$ ratio is slightly increased for $\sqrt{s_{NN}} = 6.3$ and 7.6 GeV, but the situation drastically changes for $\sqrt{s_{NN}} = 12$ GeV. The same tendency is typical of $\bar{p}/p$. On the contrary, for the $\bar{\Xi}^-/\Lambda$ ratio, there is a noticeably worse data description within the SFO $+ \gamma_s$ approach at $\sqrt{s_{NN}} = 6.3$ and 7.6 GeV. But for $\sqrt{s_{NN}} = 12$ GeV, the fit quality is sizably better compared to all previous approaches. Thus, within the present model, we re-
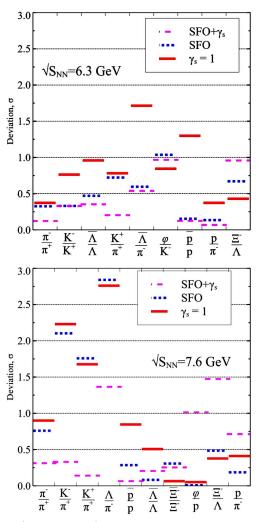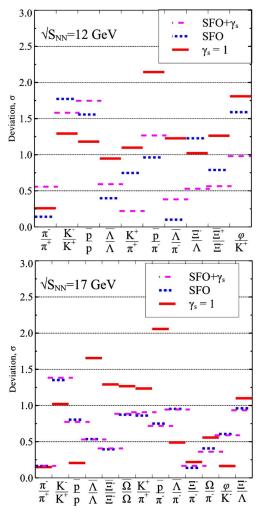


**Fig. 6.** (Colour on-line) Relative deviation of the theoretical description of ratios from the experimental value in units of the experimental error $\sigma$. Particle ratios vs. the modulus of relative deviation ($\frac{|r^{\text{theor}} - r^{\text{exp}}|}{\sigma^{\text{exp}}}$) for $\sqrt{s_{NN}} = 6.3$ and 7.6 GeV are shown. Solid lines correspond to the model with a single FO of all hadrons and $\gamma_s = 1$, the dotted lines correspond to the model with SFO. The results of a model with a combined fit with SFO and $\gamma_s$ are indicated by the dashed lines

veal a noticeable change in the trend of some ratios at $\sqrt{s_{NN}} = 7.6$–12 GeV, while, at $\sqrt{s_{NN}} = 12$ GeV, we do not observe any sizable improvement compared to the SFO model.

A special attention in our consideration was paid to the Strangeness Horn, i.e. to the $K^+/\pi^+$ ratio, because such a ratio is traditionally the most problematic one for the HRGM to fit it. As one can see from Fig. 8, the remarkable $K^+/\pi^+$ fit improvement for

**Fig. 8.** (Colour on-line) $\sqrt{s_{NN}}$ dependences of the $K^+/\pi^+$ ratio. The solid line corresponds to the results of [5]. Horizontal bars correspond to the present model with SFO $+ \gamma_s$ fit, while the diamonds correspond to the results previously obtained for SFO [7]

**Fig. 7.** (Colour on-line) Same as in Fig. 6, but for $\sqrt{s_{NN}} = 12$ and 17 GeV

$\sqrt{s_{NN}} = 2.7$, 3.3, 4.3, 4.9, 6.3, 7.6, 12 GeV justifies the usage of the present model. Quantitatively, we found that the $\chi^2/\mathrm{dof}$ improvement for the SFO $+ \gamma_s$ model is $\chi^2/\mathrm{dof} = 1.5/14$, i.e. even better than it was achieved in [7] with $\chi^2/\mathrm{dof} = 3.3/14$ for the $\gamma_s$ fitting approach and with $\chi^2/\mathrm{dof} = 6.3/14$ for the SFO model with $\gamma_s = 1$.

From Fig. 9, one can see that, at two highest RHIC energies, the description of ratios within the single FO model is very good for all ratios except for $\bar{\Lambda}/\pi^-$ at $\sqrt{s_{NN}} = 130$ GeV and for $(\Omega + \bar{\Omega})/\Xi^-$ at $\sqrt{s_{NN}} = 200$ GeV. The main reason is that, at these energies, all chemical potentials except for the strange one are almost zero, and, hence, the numbers of particles and antiparticles are almost the same. As one
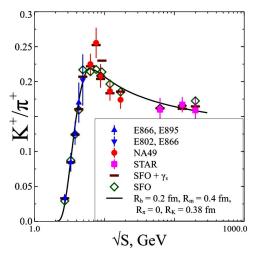
can see from the upper panel of Fig. 9, the SFO $+ \gamma_S$ fit significantly improves only the $\Omega/\pi^-$ and $\Xi^-/\pi^-$ ratios compared to the single FO model, i.e. only two ratios of strange hadrons responded to the variation of two additional parameters. For $\sqrt{s_{NN}} = 200$ GeV, the SFO $+ \gamma_S$ fit significantly improves only the $(\Omega + \bar{\Omega})/\Xi^-$ ratio and worsens the $\Lambda/\pi^-$ ratio and $\phi/p$ (less), i.e. only three ratios of strange hadrons responded to such a sophisticated fit. For $\sqrt{s_{NN}} = 62.4$ GeV, only two ratios out of five include kaons. Hence, using $T_{SFO}$ and $\gamma_s$, one can perfectly reproduce the strange particle ratios without affecting the non-strange ones. Treating the $T_{SFO}$ values found within the SFO model as an additional datum for the SFO $+ \gamma_S$ fit, we obtain the same result. Therefore, in contrast to low collision energies, only a few ratios with strange particles can be improved at high collision energies by simultaneous variation of $T_{SFO}$ and $\gamma_s$. Hence, the SFO cannot represent the majority of fitted ratios, which are well reproduced even within the single FO model with a single or with several hard-core radii. The lower panel of Fig. 5 evidently supports such a conclusion for the HRGM with the same value of hadronic hard-core radius.

Within the SFO $+ \gamma_S$ model, the $\Lambda/\pi^-$ and $\bar{\Lambda}/\pi^-$ ratios demonstrate some worsening compared to less sophisticated models. In Fig. 10, we show that the SFO $+ \gamma_S$ model does not yet improve these ra-
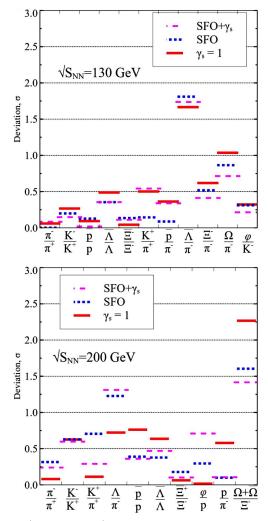
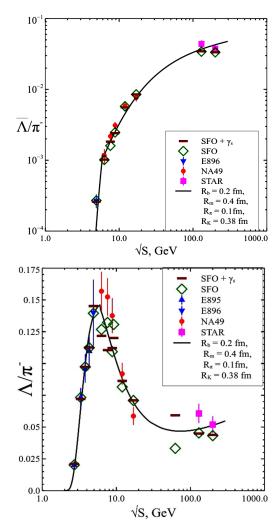**Fig. 9.** (Colour on-line) Same as in Fig. 6, but for $\sqrt{s_{NN}} = 130$ and $200$ GeV

**Fig. 10.** (Colour on-line) $\sqrt{s_{NN}}$ dependences of $\bar{\Lambda}/\pi^-$ (upper panel) and $\Lambda/\pi^-$ (lower panel) ratios. The solid line correspond to the results of a single FO model [5]. Horizontal bars correspond to the SFO + $\gamma_s$ model, while the diamonds correspond to the previously obtained results for the SFO model [7]

tios. The $\Lambda/\pi^-$ fit quality, for instance, is $\chi^2/\mathrm{dof} = 10/8$. Hence, up to now, the best fit of the $\Lambda/\pi^-$ ratio was obtained within the SFO approach with $\gamma_s = 1$. As it was mentioned in [1, 3, 5], a too slow decrease of the model results for the $\Lambda/\pi^-$ ratio compared to the experimental data is typical of almost all statistical models. Evidently, the too steep rise in the $\Lambda/\pi^-$ behavior is a consequence of the $\bar{\Lambda}$ anomaly [1,37]. Similar results are reported in Refs. [38–40] as the $\bar{p}$, $\bar{\Lambda}$, and $\bar{\Xi}$ selective suppression. Since even the introduction of the separate SFO with the strangeness enhancement factor does not allow us to better describe these ratios, we believe that there is a corresponding physical reason which is responsi-

ble for it. One of them could be a necessity to introduce the different hard-core radius $R_\Lambda$ for the $\Lambda$ (anti)hyperons [12].

## 6. Conclusions

We present a thorough investigation of the data measured at AGS, SPS, and RHIC energies within different versions of the multicomponent hadron resonance gas model. The suggested approach to separately treat the freeze-outs of strange and non-strange hadrons with the simultaneous $\gamma_s$ fitting gives

rise for the top-notch Strangeness Horn description with $\chi^2/\mathrm{dof} = 1.5/14$. The developed model clearly demonstrates that the successful fit of hadronic multiplicities includes all the advantages of these two approaches discussed in [7]. As a result, we found a significant data fit quality improvement for $\sqrt{s_{NN}} = 6.3$, 7.6, 12, 130 GeV.

At the same time, the lack of available data at $\sqrt{s_{NN}} = 2.7$, 3.3, 3.8, 4.3, 9.2, 62.4 GeV forced us to redefine the fitting procedure at these collision energies in order to avoid the mathematical inconsistency, which in combination with the large experimental error bars led to rather large uncertainties of the fitting parameters. The suggested redefinition of the fitting procedure by including the $T_{\mathrm{SFO}}$ temperatures obtained for these energies within the SFO model allowed us to avoid the mathematical problems and to get the reliable answers on the values of the residual chemical non-equilibrium of strange particles. The developed sophisticated HRGM, i.e. the SFO $+\gamma_s$ model, allowed us to describe the hadron multiplicity ratios with rather high quality $\chi^2/\mathrm{dof} = = 43.72/47 \simeq 0.93$. This very fact demonstrates that the suggested approach is a precise tool to elucidate the thermodynamics properties of hadron matter at two chemical freeze-outs. The fresh illustrations to this statement can be found in [14].

The achieved total value of $\chi^2 = 43.72$ for the SFO $+\gamma_s$ model is almost 50% lower than the $\chi^2$ value found for the single FO model and 30% lower than the SFO model $\chi^2$ value. The obtained $\gamma_s$ values are consistent with the conclusion $\gamma_s \simeq 1$ (within the error bars). An evident exception is the topmost point of the Strangeness Horn (located at $\sqrt{s_{NN}} = 7.6$ GeV), at which the mean value of the strangeness enhancement factor is $\gamma_s \simeq 1.19 \pm 0.15$. To reveal the physical reason for such a deviation, we need more experimental data with an essentially higher accuracy.

One of the main results obtained here is that the idea of the separate chemical FO of strange hadrons provides a very high quality of the data description. The further inclusion of the chemical non-equilibrium on the top of the SFO is consistent with the result $\gamma_s \simeq 1$ for all energies except for $\sqrt{s_{NN}} = 7.6$ GeV. Thus, the found residual chemical non-equilibrium of strange particles is weak. Hence, it can be safely ignored for all energies except for $\sqrt{s_{NN}} = 7.6$ GeV. The strange charge enhancement of about 20% found at this collision energy allowed us

to perfectly describe the topmost point of the Strangeness Horn, but at the expense of the worsening of the $\Lambda/\pi^-$ and $\bar{\Lambda}/\pi^-$ ratios.

In addition, the description of ratios containing the non-strange particles, especially such as $\pi^-/\pi^+$ and $\bar{p}/p$, gets better, as compared to the previously reported results [5, 7]. The remaining problem of the ratios involving the $\Lambda$ and $\Xi$ (anti)hyperons can be resolved by an inclusion of the different hard-core radius for $\Lambda$ (anti)particles [12], but such a treatment is out of scope of the present work.

The performed analysis of the SFO $+\gamma_s$ model hadronic pressures existing at FO and at SFO allowed us to elucidate an important conclusion that the single FO models with the same hard-core radius [1] or with different hard-core radii [4, 5, 7] for all hadrons reproduce the SFO pressure for all collision energies below $\sqrt{s_{NN}} = 62.4$ GeV. The main reason for such a behavior is that the number of ratios involving strange hadrons is larger than the number of ratios with non-strange hadrons.

We report also the existence of strong jumps in the SFO pressure, SFO temperature, the corresponding effective number of degrees of freedom, when the center-of-mass collision energy changes from 4.3 to 4.9 GeV. Based on the concept of non-smooth chemical freeze-out introduced recently in [14], we parametrized the dependences $T_{\mathrm{FO}}(\sqrt{s_{NN}})$ and $T_{\mathrm{SFO}}(\sqrt{s_{NN}})$, which can be verified in the future experiments planned at FAIR (GSI) and NICA (JINR). We hope that the high-precision data measured in these experiments will allow us to finally answer the question whether the residual non-equilibrium of strange charge is necessary to describe the topmost point of the Strangeness Horn or the concept of two separate chemical freeze-outs for strange and non-strange hadrons can do this without introducing the $\gamma_s$ factor.

1. A. Andronic, P. Braun-Munzinger, and J. Stachel, Nucl. Phys. A **772**, 167 (2006) and references therein.

2. J. Rafelski, Phys. Lett. B **62**, 333 (1991).

3. A. Andronic, P. Braun-Munzinger, and J. Stachel, Phys. Lett. B **673**, 142 (2009) and references therein.

4. D.R. Oliinychenko, K.A. Bugaev, and A.S. Sorin, Ukr. J. Phys. **58**, 211 (2013).

5. K.A. Bugaev, D.R. Oliinychenko, A.S. Sorin, and G.M. Zinovjev, Eur. Phys. J. A **49**, 30 (2013) and references therein.

6. K.A. Bugaev, D.R. Oliinychenko, and A.S. Sorin, Ukr. J. Phys. **58**, 939 (2013).

7. K.A. Bugaev *et al.*, Europhys. Lett. **104**, 22002 (2013).

8. S. Chatterjee, R.M. Godbole, and S. Gupta, Phys. Lett. B **727**, 554 (2013).

9. D.R. Oliinychenko, V.V. Sagun, A.I. Ivanytskyi, and K.A. Bugaev, Ukr. J. Phys. **59**, 1051 (2014).

10. G. Zeeb, K.A. Bugaev, P.T. Reuter, and H. Stöcker, Ukr. J. Phys. **53**, 279 (2008).

11. F. Becattini, J. Manninen, and M. Gazdzicki, Phys. Rev. C **73**, 044905 (2006).

12. V.V. Sagun, Ukr. J. Phys. **59**, 755 (2014) .

13. S. Chatterjee *et al.*, Adv. High Energy Phys. **2015**, 349013 (2015).

14. K.A. Bugaev *et al.*, Ukr. J. Phys. **60**, 181 (2015).

15. S. Wheaton, J. Cleymans and M. Hauer, Comput. Phys. Commun. **180**, 84 (2009).

16. J.L. Klay *et al.*, Phys. Rev. C **68**, 054905 (2003).

17. L. Ahle *et al.*, Phys. Lett. B **476**, 1 (2000).

18. B.B. Back *et al.*, Phys. Rev. Lett. **86**, 1970 (2001).

19. J.L. Klay *et al.*, Phys. Rev. Lett. **88**, 102301 (2002).

20. C. Pinkenburg *et al.*, Nucl. Phys. A **698**, 495c (2002).

21. S. Albergo *et al.*, Phys. Rev. Lett. **88**, 062301 (2002).

22. P. Chung *et al.*, Phys. Rev. Lett. **91**, 202301 (2003).

23. S.V. Afanasiev *et al.*, Phys. Rev. C **66**, 054902 (2002).

24. S.V. Afanasiev *et al.*, Phys. Rev. C **69**, 024902 (2004).

25. T. Anticic *et al.*, Phys. Rev. Lett. **93**, 022302 (2004).

26. S.V. Afanasiev *et al.*, Phys. Lett. B **538**, 275 (2002).

27. C. Alt *et al.*, Phys. Rev. Lett. **94**, 192301 (2005).

28. S.V. Afanasiev *et al.*, Phys. Lett. B **491**, 59 (2000).

29. B. Abelev *et al.*, Phys. Rev. C **81**, 024911 (2010).

30. B. Abelev *et al.*, Phys. Rev. C **79**, 034909 (2009).

31. J. Adams *et al.*, Phys. Rev. Lett. **92**, 182301 (2004).

32. J. Adams *et al.*, Phys. Lett. B **567**, 167 (2003).

33. C. Adler *et al.*, Phys. Rev. C **65**, 041901(R) (2002).

34. J. Adams *et al.*, Phys. Rev. Lett. **92**, 112301 (2004).

35. J. Adams *et al.*, Phys. Lett. B **612**, (2005) 181.

36. A. Billmeier *et al.*, J. Phys. G **30**, S363 (2004).

37. B.B. Back *et al.*, Phys. Rev. Lett. **87**, 242301 (2001).

38. F. Becattini *et al.*, Phys. Rev. C **85**, 044921 (2012).

39. F. Becattini *et al.*, Phys. Rev. Lett. **111**, 082302 (2013).

40. J. Stachel, A. Andronic, P. Braun-Munzinger, and K. Redlich, arXiv:1311.4662 [nucl-th].

41. K.A. Bugaev *et al.*, Phys. Part. Nucl. Lett. **12**, 238 (2015).

*К.О. Бугаєв, Д.Р. Олійниченко, В.В. Сагун,*
*О.І. Іваницький, Ж. Клейманс, Є.С. Мирончук,*
*Е.Г. Ніконов, А.В. Тараненко, Г.М. Зінов'єв*

ОКРЕМІ ФІЗИЧНІ ФРІЗАУТИ ДИВНИХ
ТА НЕДИВНИХ АДРОНІВ ТА ПРОБЛЕМА
ЗАЛИШКОВОЇ ХІМІЧНОЇ НЕРІВНОВАГИ
ДИВНОСТІ В РЕЛЯТИВІСТСЬКИХ
ЗІТКНЕННЯХ ВАЖКИХ ІОНІВ

Р е з ю м е

Запропоновано покращену версію моделі адронного резонансного газу, яка розглядає окремий хімічний фрізаут дивних і недивних адронів в комбінації з додатковим фактором $\gamma_s$, який враховує залишкову хімічну нерівновагу дивних частинок. У рамках запропонованого підходу параметри двох хімічних фрізаутів пов'язані законами збереження ентропії, баріонного заряду, третьої проекції ізоспіну та дивності. Розвинута модель дозволила провести високоякісний фіт відношень множинностей адронів, що вимірювались на прискорювачах AGS, SPS і RHIC з $\chi^2/\text{dof} \simeq 0{,}93$. Особливу увагу було приділено успішному опису піка дивності. Добре відому проблему селективного пригнічення $\bar{\Lambda}$ та $\bar{\Xi}$ гіперонів також обговорено. Головний результат полягає в тому, що в межах помилок $\gamma_s$ фактор дорівнює одиниці для всіх енергій зіткнення, крім енергії зіткнення в системі центра мас 7,6 ГеВ, за якої знайдено підсилення дивності на 20%. Також виявлено існування сильних стрибків в тиску, температурі та ефективній кількості ступенів вільності на стадії хімічного фрізаута дивних частинок, коли енергія зіткнення в системі центра мас змінюється від 4,3 до 4,9 ГеВ. Приведено аргументи на користь того, що ці нерегулярності можуть бути сигналом кварк-адронного фазового переходу.